Bio-Design and Manufacturing (2020) 3:87–97
https://doi.org/10.1007/s42242-020-00071-x

RESEARCH ARTICLE

Standing surface acoustic wave-assisted fabrication of patterned microstructures for enhancing cell migration

Yancheng Wang[1,2] · Yue Wang[2,3] · Deqing Mei[1,2] · Zongkai Yu[2] · Dai Xue[2]

Received: 20 February 2020 / Accepted: 4 April 2020 / Published online: 18 April 2020

Abstract

Microfluidic device with patterned microstructures on the substrate surface was used to regulate cell adhesion, morphology, and functions in tissue engineering. We developed a microfluidic device which employing microscale patterned microstructures to achieve enhanced cell adhesion and migration. Biocompatible hydrogel substrates with micro-wavy and lattice-patterned microstructures were fabricated using standing surface acoustic waves and ultraviolet solidification. After seeding the L929 mouse fibroblast cells onto the patterned substrate of the microfluidic device, we determined that the viability and proliferation rate of cell migration can be greatly enhanced. Furthermore, L929 cells showed two types of gathering modes after 48 h of culturing. Cell growth was guided by the patterned substrate used in the microfluidic device and showed differences in the location distribution. Therefore, the developed microfluidic device with patterned microstructures can extend the application of in vitro cell culturing for future drug development and disease diagnosis.

Keywords Standing surface acoustic waves (SSAWs) · Micropatterned structure · Dynamic cell culture · Microfluidic device

Introduction

Cell culturing models can mimic cell microenvironment in vivo to provide carriers and channels for the growth of tissue and migration of cells. The development of in vitro cell culturing model is a technical challenge and has several applications in tissue engineering such as in drug delivery [1], specialized diagnosis, and biological research [2, 3]. Traditional cell culturing implies the seeding of cells in petri dishes or microplates with a specific nutrient solution. Dynamic cell culturing using a user-defined microfluidic chip/device with fluid flow allows to circulate nutrition and remove metabolic waste, which may enhance cell migration and proliferation rate in cell culturing. Nupura et al. [4] have proposed a liver-on-a-chip device, which allows a continuous access to cells for a long period of culturing time, which enables the direct bioprinting of hepatocyte spheroid-laden hydrogel constructs. Toh et al. [5] have developed a 3D microfluidic hepatocyte chip for in vitro drug toxicity testing with the aim to predict drug hepatotoxicity. The developed microfluidic hepatocyte chip contains multiple microscale fluidic channels, which creates a 3D cell microenvironment to maintain the synthetic and metabolic function of hepatocytes. Similarly, Zhang et al. [6] have presented a multi-channel 3D chip for the culturing of four different types of cells to mimic human organs such as liver, lung, kidney, and fat.

Though microfluidic devices are capable of substance exchange, they are limited in mimicking the in vivo microenvironment because microfluidic devices cannot reduce three-dimensional structures such as cells grown in an in vivo environment. Therefore, several methods have been proposed for the fabrication of biomimetic microstructures for the development of cell-culturing microfluidic devices. To mimic the mineral components and microstructures of natural bones, Wei et al. [7] have fabricated polymer-based composite scaffolds with architecture that is designed for

Electronic supplementary material The online version of this article (https://doi.org/10.1007/s42242-020-00071-x) contains supplementary material, which is available to authorized users.

✉ Yancheng Wang
yanchwang@zju.edu.cn

1 State Key Laboratory of Fluid Power and Mechatronic Systems, School of Mechanical Engineering, Zhejiang University, Hangzhou 310027, China

2 Key Laboratory of Advanced Manufacturing Technology of Zhejiang Province, School of Mechanical Engineering, Zhejiang University, Hangzhou 310027, China

3 Department of Aerospace and Mechanical Engineering, The George Washington University, Washington, DC 20052, USA

cell attachment and migration in bone tissue engineering. In addition, they determined that using the artificial hexagonal lobule unit structure, hepatic cells improved morphological organization with higher liver-specific gene expression levels and increased metabolic product secretion [8]. Johan et al. [9] have utilized a multi-material 3D printing process to fabricate the cardiac micro-physiological device, which contains the wavy-shaped surface with the aim to guide the self-assembly of engineered cardiac tissue. Thus, dynamic cell culturing based on 3D architecture scaffolds has been proven to be an effective method to enhance cell culturing and tissue integration in a lab-on-chip microfluidic device.

Owing to the slogan "smaller brings new capability" [10], the patterned microstructure fabrication has received considerable attention. Compared to the ultra-precision machining techniques for metal or hard material fabrication [11], polymer-based patterned microstructure fabrication has made considerable progress over the past decade. Kaufmann et al. [12] have presented "sandwich" micro-contact printing to fabricate patterned structures to prepare Janus polymer micro-particles. Tang et al. [13] have developed a novel micro-molding process using the vacuum casting technique; the micro-gear was fabricated functionally and reproducibly. Three-dimensional (3D) printing processes (e.g., direct ink writing [14], stereolithography [15, 16], extrusion-based printing [17], inkjet printing [18, 19], and electrospinning [20]) have been applied to fabricate polymer-based microscale objects. Nevertheless, most of these processes require additional user-defined mold design and fabrication. Also, the demolding procedure of these fabrication processes may introduce several defects on the final fabricated microstructures, thus would limit the application of these processes in the fabrication of complex constructs.

Here we propose a novel method to fabricate polymer-based patterned microstructures with the assistance of standing surface acoustic waves instead of using the physical mold. Surface acoustic waves (SAWs), generated by applying sinusoidal signals to interdigital transducers (IDTs), can propagate along the elastic surface [21]. After standing SAWs encounter a liquid film on the substrate, a stable pattern can be created on the liquid surface that can be cured by ultraviolet (UV) solidification [22]. Compared with traditional fabrication processes, the SAW-assisted fabrication process mainly has two advantages: (1) free-form fabrication without using the physical mold, thus demolding procedure is not required, and the defects induced by demolding can also be eliminated; (2) the cost fabrication time is quite short and usually less than 2–3 s. The entire fluid film will be deformed to generate the patterned microstructures by using the excitation of standing SAWs; the deformed fluid film is then curved by UV exposure.

Furthermore, the standing SAW-assisted fabrication process introduces only low-power mechanical vibrations to the suspension and utilizes the ultrasonic energy field that produces the vibration of the light-sensitive liquid film and undulates the surface with different patterns [23]. In terms of material selection, the UV-sensitive materials, e.g., polyethylene glycol (PEG) [24], poly (caprolactone) (PCL) [25, 26], and their copolymers [27, 28], could be used. Here, polyethylene glycol diacrylate (PEGDA) was selected as the material for the substrate of microfluidic device owing to its superior biocompatibility [29]. In this study, we used standing SAWs to fabricate a biocompatible polymer-based substrate with undulated patterned microstructures to develop a microfluidic device; we used this substrate to guide the L929 mouse fibroblast cell growth in terms of proliferation and distribution.

Materials and methods

Materials synthesis and preparation

A biocompatible photo-sensitive liquid PEGDA mixture is utilized. It is made of 90% (wt/vol) PEGDA (number average molar mass Mn = 700, Sigma, USA), 9.5% (wt/vol) phosphate buffer saline (PBS, MULTICELL), and 0.5% (wt/vol) lithium phenyl-2,4,6-trimethylbenzoylphosphinate (LAP, Sigma, USA). These solutions were evenly mixed using ultrasonic stirring for 20 min. The photo-initiator (LAP) was synthesized by following our previous work [30]. First, the solution of ethyl(2,4,6-trimethylbenzoyl) phenylphosphinate (0.04 mol, Sigma, USA) was added to the mixed solution of lithium bromide (0.04 mol, Sigma, USA) and pure 2-butanone (227 mL, HUSHI). Then, the mixture was heated to 50 °C for 40 min until a white precipitate was generated. Then, the mixture was cooled to room temperature and kept away from light for 4 h. Next, the solution was filtered, and the solid precipitate was washed with 2-butanone three times to remove unreacted lithium bromide. Then, the filtrate was transferred to a vacuum oven to remove residual 2-butanone. Finally, PEGDA and LAP were dissolved in DPBS at the final concentration of 20% (v/v) PEGDA and 0.5% (w/v) LAP.

The photo-sensitive polymer used here polymerizes via free-radical-based photopolymerization, where incident UV light causes free-radical generation from the photo-initiator LAP, as in Fig. 1a. The generated free radicals induced carbon–carbon double chain break and activate PEGDA monomers to form cross-linked PEGDA. The polymerization of two or more monomer units polymerized into the macromolecular monomer polymerization, as shown in Fig. 1b. Thus, the liquid pre-polymer PEGDA can be photopolymerized into a solid state through these two reactions.

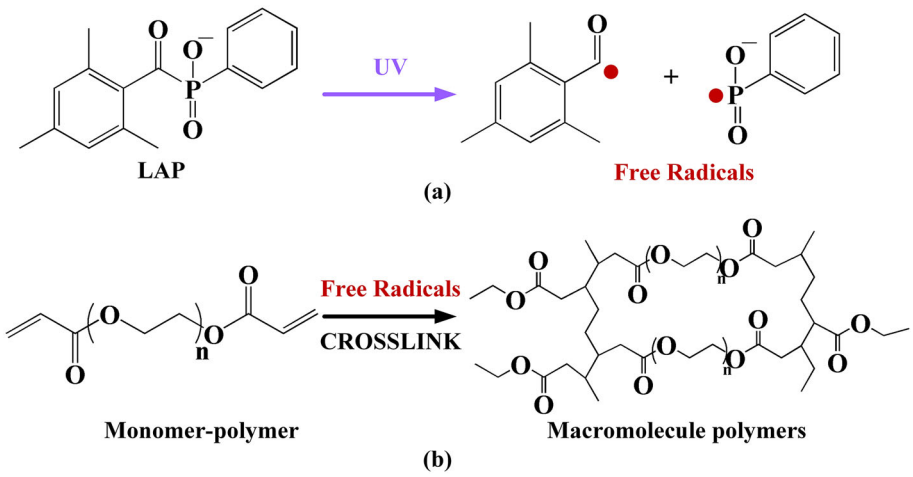

Fig. 1 **a** Schematic view of the LAP cleavage into substituent radicals after photon absorption; **b** free-radical-induced cross-linking of PEGDA monomers

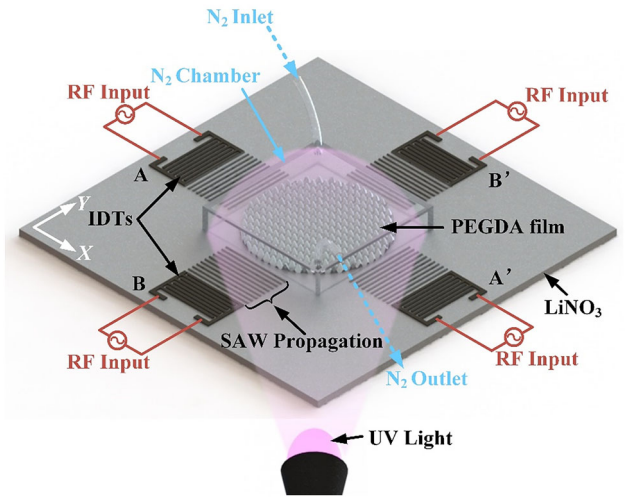

Fig. 2 Standing SAW (SSAW) generated on the $LiNbO_3$ substrate and the superposition of SSAWs to generate lattice pattern on the PEGDA film surface. PEGDA with a patterned surface was cured when exposed to UV light in an N_2 atmosphere

SSAWs-assisted fabrication method

SAW can propagate along the piezoelectric substrate and causes the deformation on the surface of liquid film. The patterned microstructure is acquired by curing the SAW-excited stable patterns on the photo-sensitive pre-polymer surface, as shown in Fig. 2. More importantly, the patterned microstructures can be adjusted by selecting different SAW working parameters such as input voltage, working frequency, and the pair number of working IDTs [31, 32].

According to our previous work, the width of the undulate pattern was equal to the half value of the wavelength of SSAW that was excited by IDTs. The width and gap distance of the structural designed electrodes of the IDTs usually determine the working frequency of the SAWs and their wavelength. For the excited patterned stripes, the period of the undulated stripe pattern was equal to the half value of the wavelength of the standing SAW. Therefore, the structure of the electrodes of the IDTs, such as width and gap distance, will determine the final fabricated period of the undulated stripe patterns. The velocity of sound wave in the $LiNbO_3$ substrate is approximately 3920 m/s, and the working frequency was equal to the wave velocity divided by the wavelength. The wave length of SAW was determined by the width of the designed IDTs, which was four times the width of the interdigital electrode. Typically, to fabricate undulate patterned strips with 70-μm spacing, the length of SAW is 140 μm, which means that the designed width of IDTs should be 35 μm. These parameters are used to design and fabricate the SAW device.

Fabrication of patterned microstructures

The setup for the fabrication of patterned microstructures is shown in Fig. 3; the SAW device is placed on top of a 2-axis manual linear stage. A UV light with a 365-nm wavelength and 10-W power is placed underneath the SAW device as it shown in the upper right corner of Fig. 3. An industrial camera (XDS-0745) with a display screen is connected to observe the working region of the SAW device in real time, as shown in Fig. 3. Because the designed SAW device has two pairs of IDTs, two waveform generators (Agilent 33522B, Tektronic AFG 3052C) are used to generate sinusoidal signals on IDTs. To enhance the amplitude, two power amplifiers (Mini-Circuits ZHL-1-2 W+) are connected between the waveform generator and SAW device. At the same time, a stabilized voltage supply with 24 V is used to provide power-to-power amplifiers.

Because the designed SAW device has two pairs of orthogonally arranged IDTs, we have two types of IDTs for the fabrication of patterned microstructures: to use one-pair IDTs (A–A′ or B–B′) or to use two-pair IDTs (A–A′ and B–B′). For each type of selection, a four-step procedure is used to

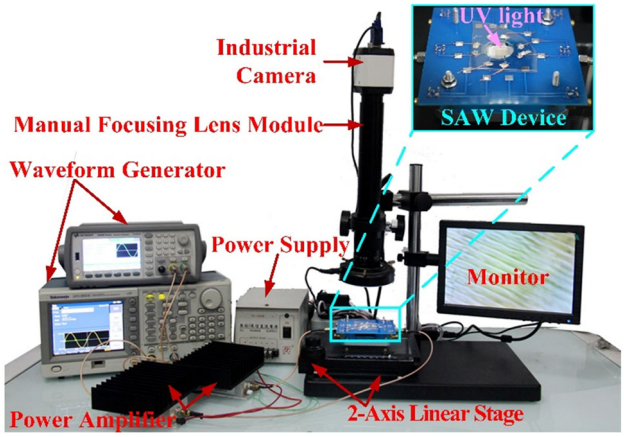

Fig. 3 Experimental setup of the SSAW-assisted fabrication process

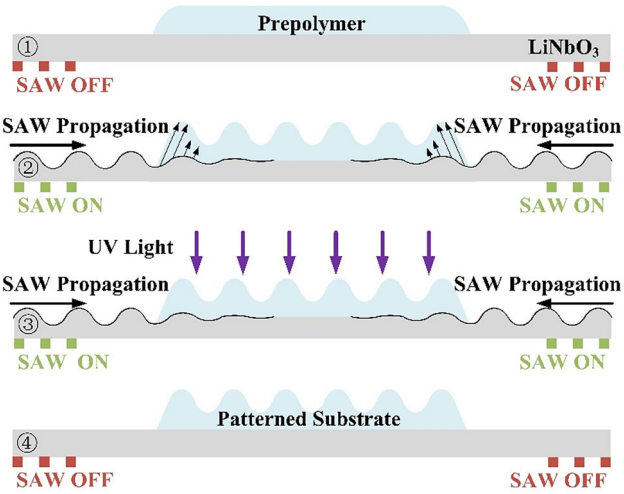

Fig. 4 Flow diagram of the four-step procedure for the fabrication of patterned microstructures

fabricate the patterned microstructures, as shown in Fig. 4. Step 1: a thin layer of liquid PEDGA pre-polymer was placed at the center of the SAW device using a micropipette. The thickness of the PEGDA film was controlled to be approximately 30–50 μm. Step 2: the power amplifier and waveform generator were turned on. Sinusoidal signals were generated, amplified, and input into IDTs to excite SAW. Then, the patterned surface can be excited on the pre-polymer liquid film. Step 3: after the stabilization of the pre-polymer, the UV light was used to solidify the patterned surface under an oxygen-free atmosphere. The time duration of solidification requires approximately 3 s. Step 4: the UV light, waveform generator, and power amplifier are turned off; the PEGDA film with a patterned microstructure was peeled off from the SAW device using tweezers.

After fabrication, a laser scanning confocal microscope (OLS4100, Olympus) is used to measure the morphology of the patterned microstructures. By selecting one or two pairs of IDTs, it is possible to fabricate different patterned substrates. Using one-pair of IDTs, it is possible to excite a micro-wavy pattern on the liquid film surface, and an undulated stripe pattern can be fabricated; when using two pairs of IDTs at the same time, two perpendicular waves are superimposed, and the lattice-pattern can be obtained.

Because L929 cells will grow and proliferate with attaching, the fabricated patterned microstructures were soaked in 300 μL of the collagen solution with the concentration of 1 mg/mL for 4 h as a pre-treatment. For sterilization, the patterned microstructures were exposed to UV light for 4 h and then washed twice with PBS to remove excess collagen.

Cell culturing device design and fabrication

The designed structure of the microfluidic device for cell culturing consists of three layers. Specifically, the top microfluidic layer is used for fluidic channels, the bottom-well layer is used for cell adherence culture, and the glass slide is used for the successive encapsulation from top-down, as shown in Fig. 5a. The top microfluidic layer is used for the import and export of the cell culture medium. The bottom-well layer was attached to the glass slide, and the wells between the bottom-well layer and the glass slide were used as cell culture chambers, where the fabricated patterned microstructure substrates were attached. The bottom-well layer was also used for the import and export of the cell suspension.

For the fabrication of the cell culturing device, both the top microfluidic layer and the bottom-well layer were fabricated by the casting process using the thermo-curing material. This material was prepared using a thermosetting resin polydimethylsiloxane (PDMS, DOW CORNING, Sylgard 184) and a curing agent at the ratio of 10:1. After stirring and vacuum defoaming for 2 h, the mixture was poured into the SLA printed mold and then put into a vacuum drying oven to shape. To enhance the integral mechanical properties of the cell culturing device, the curing temperature needs to be strictly controlled. In this study, the curing temperature in the vacuum oven was set to 65 °C, and the time required to fully cure and semi-cure the top microfluidic and bottom-well layers was 60 min and 45 min, respectively.

For the bonding and encapsulation of the device, the bottom-well layer was first bonded with the glass slide using the viscosity of the semi-cured surface, and the aligned double layers were put into the vacuum oven for 2 h to fully cure PDMS and to generate a strong bond between the bottom-well layer and the glass slide. Second, the patterned microstructure substrates were put into the cell culture well, and each culture well had one piece of the patterned substrate. Third, the joint surfaces of the top microfluidic layer and the bottom-well layer were processed by oxygen plasma treatment for 50 s. Then, the top microfluidic layer and the bottom-well layer were quickly bonded. These three layers

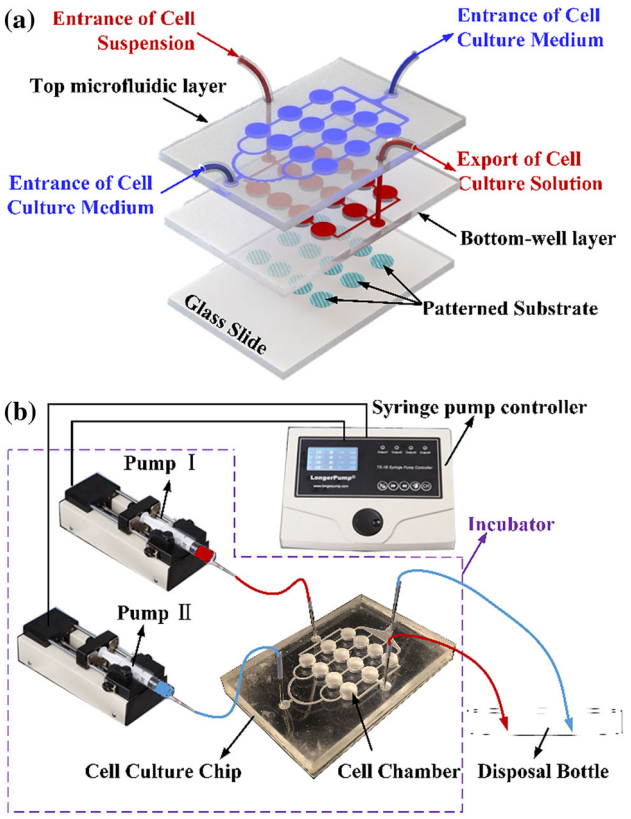

Fig. 5 **a** Design of the three-layered cell culturing microfluidic device on the basis of the patterned microstructure substrates. **b** Schematic diagram of pumping and dynamic cell culturing. A syringe pump controller is used to control two pumps in the microfluidic device with different pumping velocity and time

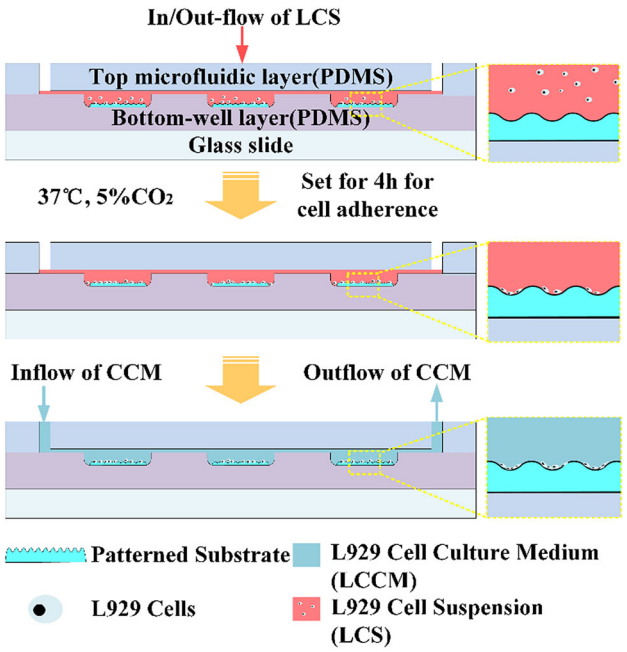

Fig. 6 Dynamic cell culturing in the developed three-layered microfluidic device

were clamped and placed at room temperature for 12 h for encapsulation. Finally, four stainless-steel needles, with the inner and external diameters of 0.8 mm and 1.0 mm and the length of 20 mm, were inserted into the top microfluidic layer and served as the import and export locations of cell suspension and culture medium. The connection between the microfluidic device, pumps, and its controller are shown in Fig. 5b.

Cell culturing and the evaluation of cell growth

To demonstrate the performance of the fabricated patterned microstructures of the developed microfluidic device, cell culturing experiments were conducted. First, L929 mouse fibroblasts were cultured in MEM (Tangpu Biological Technology Co., Ltd., HangZhou, China) with a 10% fetal bovine serum (Tangpu Biological Technology Co., Ltd., HangZhou, China), 1% penicillin (100 units/mL), and streptomycin (100 μg/mL) (Tangpu Biological Technology Co., Ltd., HangZhou, China). The prepared cells were maintained in an incubator at 37 °C with 5% CO_2. Before cell seeding and perfusing, the injection pump, injector, needles and patterned substrates were filled or immersed in a 75% ethanol solution under UV exposure for 1 h and subsequently washed with sterile PBS three times.

The medium was changed every 2 days, and L929 cells were passaged by trypsin–EDTA (Tangpu Biological Technology Co., Ltd., Hangzhou, China) dissociation at 90% confluence every 4 days. The cell suspension was prepared at the density of 5×104 cell/mL for seeding and perfusing. For comparison, both static cell culturing and dynamic cell culturing were performed. In static cell culturing, 24-well plates were used. The polymer-based substrates with patterned microstructures were placed and attached to the bottom of the well. For comparison, a blank well without a patterned substrate was used as the static 2D culturing group. Each group had 6 culture wells, and 1 mL of the previously prepared cell suspension was added to each well with a pipette.

During dynamic cell culturing, the prepared cell suspension was cultured in the microfluidic device. As shown in Fig. 6, the imports and exports were connected with PTFE pipes. One syringe, containing 3 mL of the cell suspension, was connected with an inject pump I that was connected with an import, as shown in Fig. 5b. The other syringe, containing 10 mL of the MEM medium, was connected with the other injector pump II that was connected with the bottom-well layer import. The exports of both two layers were connected with the disposal bottle. After connecting all pipes, pump I was turned on at the ratio of 1 mL/min, and the cell suspension was pumped into wells. After 1 min, the wells were

seeded with cells, and the cell culturing device was placed into an incubator for 4 h until the cells grew on the walls. Then, pump II was turned on, and the medium was continuously pumped at the ratio of 125 L/h.

Cell viability analysis

Cell viability was examined using the LIVE/DEAD assay reagents (KeyGENBioTECH Co., Ltd., Nanjing, China). Calcein acetoxymethyl ester (calcein AM) and ethidium homodimer-1 were diluted with PBS to the concentrations of 2 μM and 8 μM, respectively. Calcein AM is retained within live cells and produces an intense uniform green fluorescence; ethidium homodimer enters cells through damaged membranes and produces a 40-fold enhancement of fluorescence upon binding to nucleic acids to produce bright red fluorescence in dead cells. After 40 min, the reagents were aspirated and the filaments were washed by PBS to remove the residual regents. The filaments were imaged using confocal fluorescence microscopy (ZEISS LSM780) to acquire two images of each frame; red and green marks indicate live and dead cells, respectively.

Cell proliferation and adherence analysis

L929 cells can grow by adhering to the wall and proliferate in vitro. The attached cells have a spindled-like shape, while cells that are not attached are spherical. According to this shape difference, a MATLAB program was designed to distinguish whether the cells were attached or not and to count the number of spherical and spindle cells. At first, the cell growth diagram was imaged using optical confocal microscopy (OLS4100, OLYMPUS). Then, the images were transferred into gray-scale images, and the contrast was increased. Then, gray-scale images were transferred to binary images using the adaptive threshold value method for morphological processing. Finally, the cell number could be counted.

Statistical analysis

All values were presented as the mean ± standard deviation (SD). A one-way analysis of variance (ANOVA) with t test was used to verify statistically differences among groups. The differences with p values ($p < 0.05$) were considered statistically significant. Data are presented as the mean ± standard deviation, $n \geq 9$, $^{*}p < 0.05$, $^{**}p < 0.01$.

Results and discussion

Fabrication of polymer-based patterned microstructures

Using the SSAW-assisted fabrication method, the polymer-based periodic microstructure was fabricated. Figure 7a, b and e, f show the fabricated results of 2D and 3D stripe patterned substrates when using one pair of IDTs, respectively. Figure 7a shows that the blue part was the stripe valley with a width of approximately 70 μm, this value was consistent with the designed SAW device, and the wavelength was set to be 140 μm. Figure 7b shows that the width of the stripe valley was approximately 100 μm when the wavelength of the SAW device was set as 200 μm. The amplitudes of both two stripe patterned substrates are about 35–40 μm. The green part was the crest that could offer a "wall" for cell proliferation. As in Fig. e and f, the differences between the width of stripe patterned microstructures can be observed easily under the microscope. The bright and dark parts are the top surface and valley of the stripe microstructures, respectively.

When using two pairs of IDTs, the lattice patterned microstructures were fabricated and shown in Fig. 7c, d and g, h. The lattice patterned microstructure can be regarded as the composition of two perpendicular stripe patterned substrates. The period of lattice patterned microstructures has the approximate width and height values that are similar to those of the stripe patterns because the same parameters of the SAW device and IDTs were used. Figure 7c shows the 3D view of the valley with a 70 μm wide lattice substrate, while Fig. 7d offers 100 μm one. Similarly, the differences between 2D images as in Fig. 7g and h can be observed easily. The bright part was the top surface of the lattice microstructure, which was the green part in Fig. c and d. Meanwhile, the dark part was the valley bottom, which was the blue part as in Fig. c and d. The results demonstrated that the period of the patterned microstructures can be customized by adopting specific IDTs.

Cell viability and proliferation for static and dynamic cell culturing

To validate the improvement of cell viability and cell proliferation when cells are cultured in the developed microfluidic device, three sets of experiments were conducted: static 2D culturing, static 3D culturing, and dynamic 3D culturing. Compared to traditional static culturing, dynamic cell culturing offers more chances for cells to assess the nutrition and exchange the metabolic waste.

By analyzing cell viability and proliferation mentioned before, we obtained the images of the fluorescence microscopic bioassay with L929 cells when using static 2D culturing, static 3D culturing, and dynamic 3D culturing, as

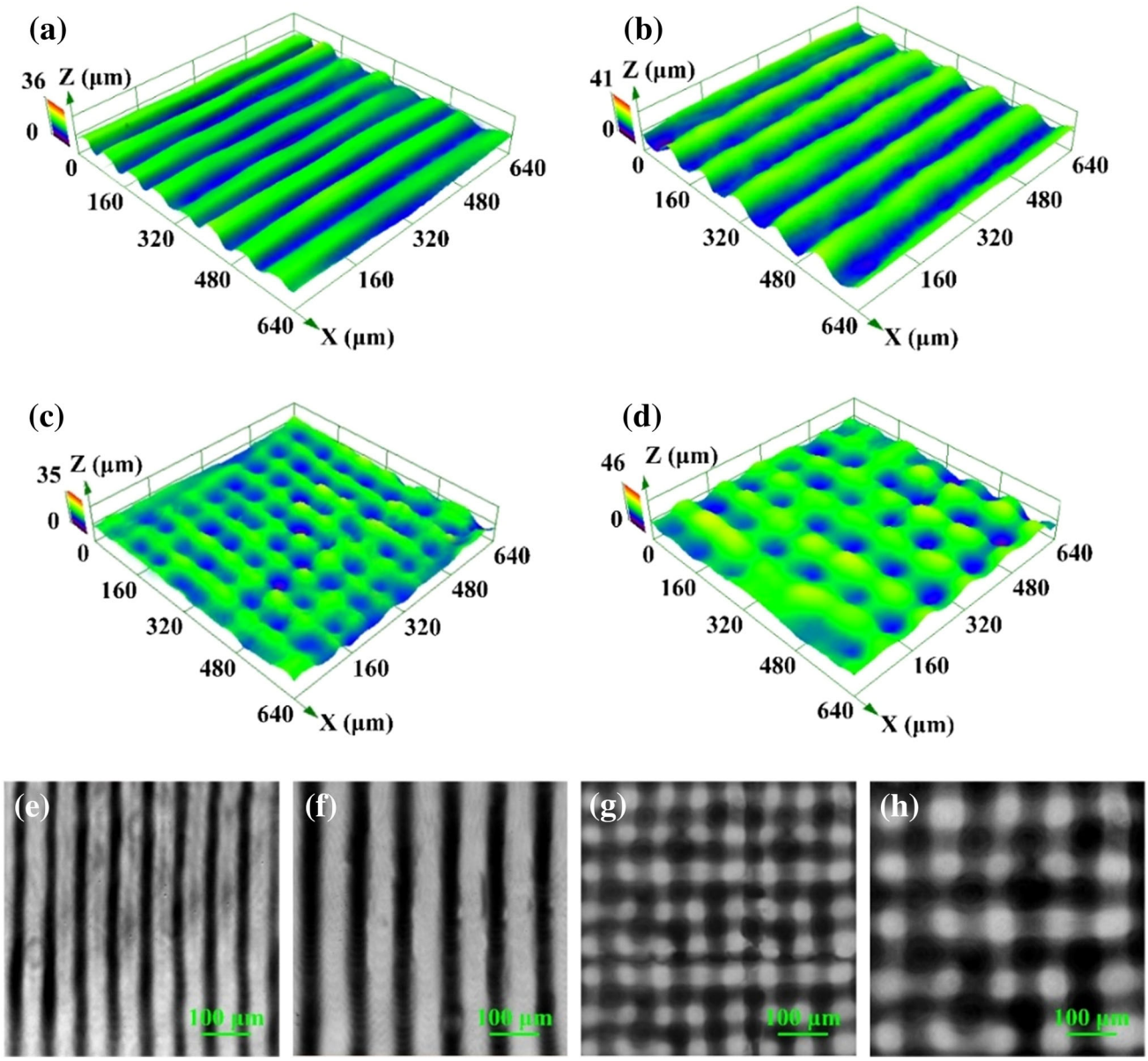

Fig. 7 Fabrication results of the microstructures: 3D stripe pattern with a width of **a** 70 μm and **b** 100 μm (**b**); 3D lattice patterns with a width of **c** 70 μm and **d** 100 μm; **e**–**h** are their 2D morphologies

shown in Fig. 8a–c. 3D dynamic culturing showed a clear advance compared to that of the static 2D culturing and static 3D culturing both in viability and proliferation after 24 h of culturing. In addition, the cell viability is shown in Fig. 8a and b; there was benefit when using 3D culturing. We used the MATLAB program to count the cell number under these three sets of experiments; an increase in the cell number is plotted in Fig. 8d. The viability of L929 cells after 48 h of culture was 92.6 ± 0.7% in static 2D culturing; in static 3D culturing, the value was 93.1 ± 1.2%; in dynamic 3D culturing, the value was 97.3 ± 1.1%. Clearly, it was observed that an increase in the cell number under 3D dynamic culturing was more significant than that of static culturing (approximately 5%). In addition, by comparing Fig. 8a and b, there existed cell morphology differences in cell distribution. Thus, the feasibility of using the designed microfluidic device was confirmed, and cell proliferation was observed.

Furthermore, the differences between 2D and 3D cell culturing on cell attachment angle distribution have been compared and shown in Fig. S1. Details can be found in Supporting Information. As in Fig. S1, the cells showed certain alignment along with the stripe substrates when using 3D culturing method. Especially in 3D dynamic culturing, more than 55% of cells had the best alignment and were

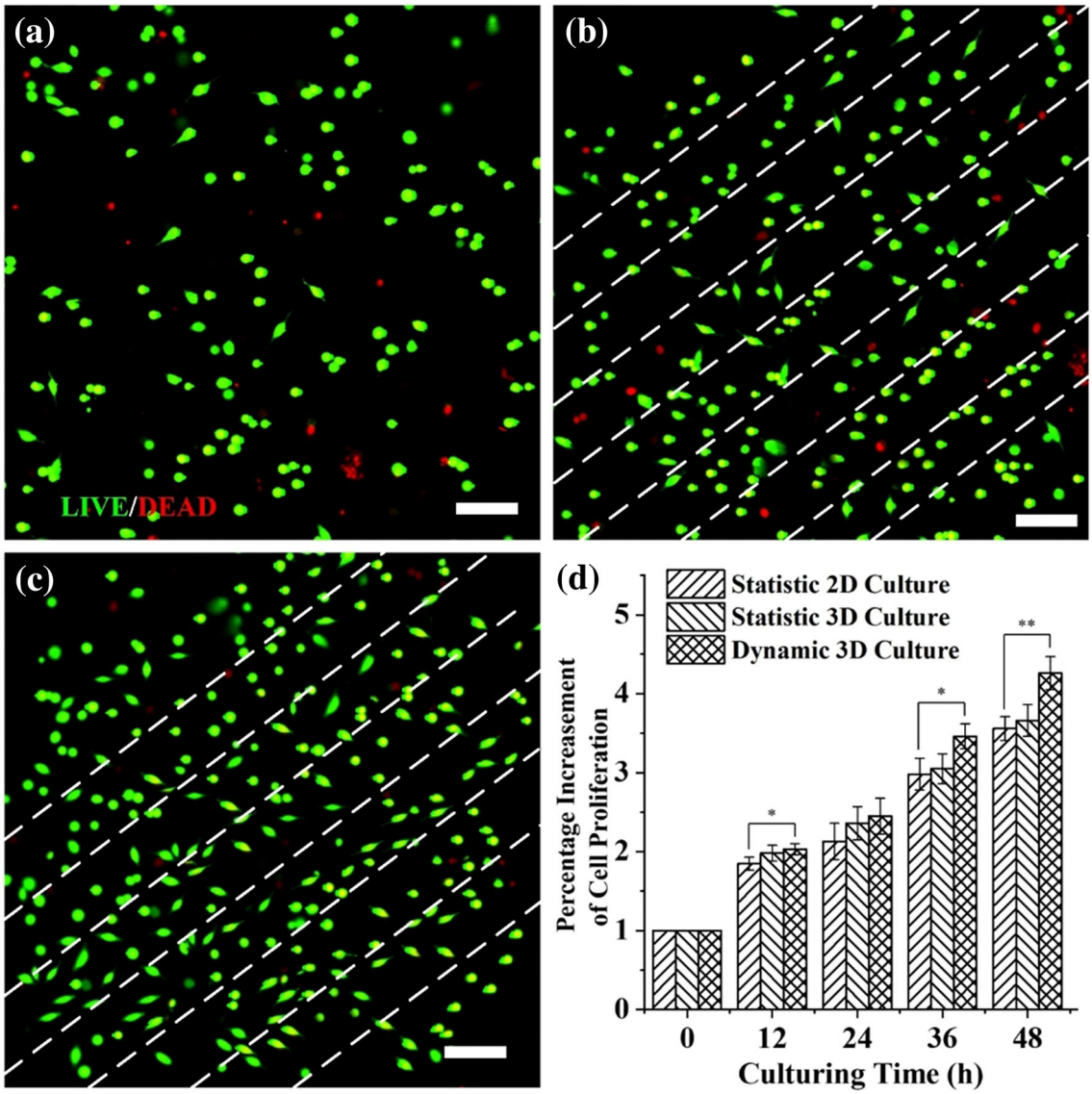

Fig. 8 Cell proliferation under different culturing methods. Images of fluorescence-stained L929 cells after 24 h of culturing under **a** static 2D culturing, **b** static 3D culturing, **c** dynamic 3D culturing; **d** the percentage increase in cell proliferation under three different culturing methods after 0, 12, 24, 36, and 48 h. Data are presented as the mean ± standard deviation, $n \geq 9$, $^{*}p < 0.05$, $^{**}p < 0.01$. (*Living cells were dyed green, and dead cells were dyed red.)

attached to the strip substrate within 30°. Meanwhile, for 2D culturing, cells attached randomly and less than 40% of cells were attached to the stripe substrates among 0°–30°. Thus, we can conclude that 3D culturing can help cells proliferate along with designed stripe substrates. Besides, we compared the differences between three types of culturing methods; the ratio was equal to the number of spindle-like cells divided by the total cell number. As shown in Fig. S2, it indicated that 3D dynamic culturing performed better in helping cells proliferate from the spheroidal phenotype to spindle-like ones.

Cell distribution on stripe/lattice patterned microstructures

To ensure that cells can attach to the PEGDA surface, we put the fabricated patterned microstructures into the collagen solution for pre-treatment, as mention before. After seeding, L929 mouse fibroblast cells had spherical or ellipsoidal shapes, as shown in Fig. 9a and d. The seeded cells tend to sink to the valley of the strip pattern owing to gravity, where cells gather in the valley, which is shown as the blue dashed line in Fig. 9a and d. In contrast, in the white line guided part, which we named wave crest, hardly any cells

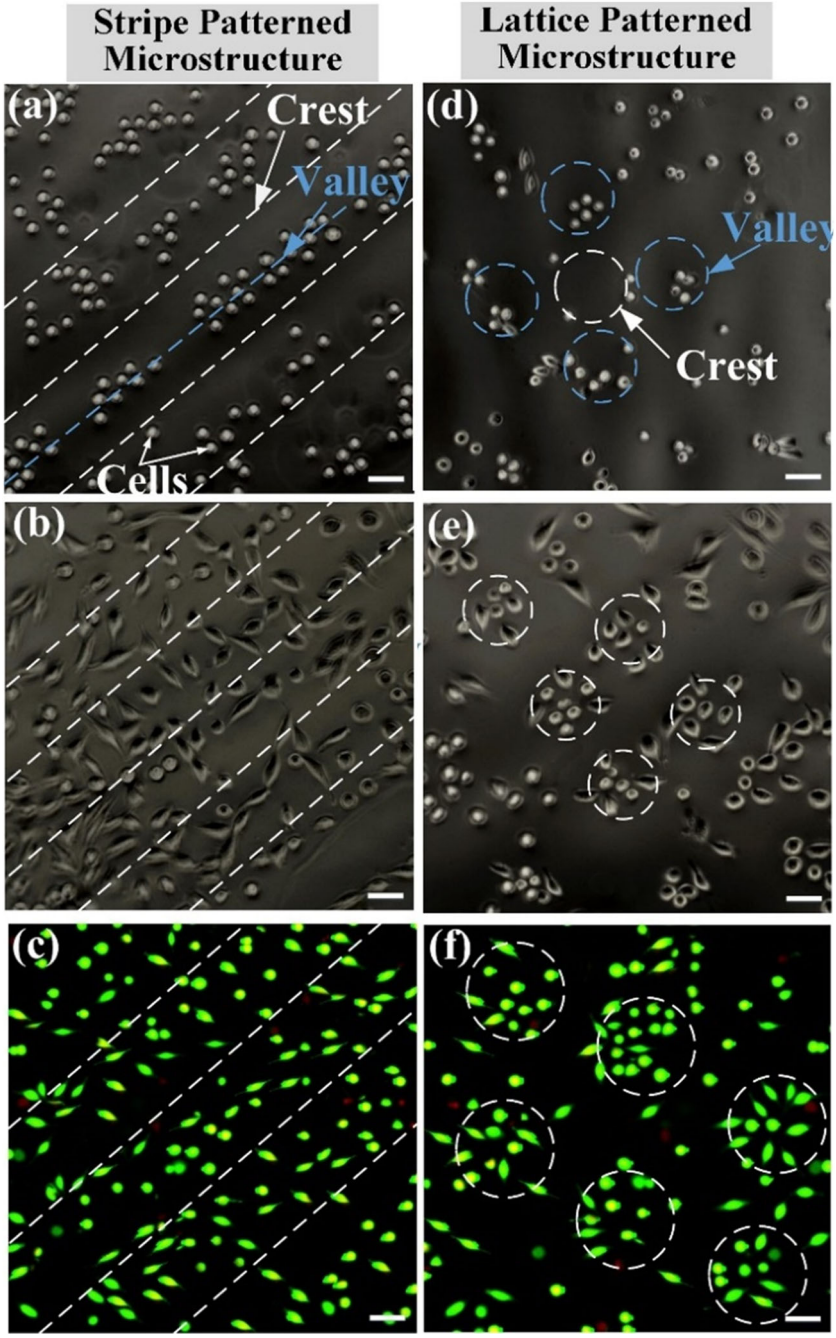

Fig. 9 24 h after cell seeding on **a** stripe patterned substrate and **d** lattice patterned substrate; the cells were seeded into the valleys as (**b**) and (**e**). After 48 h, the cells are attached along the valley of the patterned substrates. **c** and **f** are images of fluorescence-stained L929 cells after 48 h of dynamic culturing. Cells were proposed by LIVE/DEAD kit, while live is green and dead is red. *Scale bar is 50 μm

gathered, as shown in Fig. 8a–d. We can see that most cells were distributed along the valley in the stripe patterned substrate. After 48 h, a clear cell proliferation can be observed, and most cells were attached to the patterned substrate with a spindled shape, as shown in Fig. 9b–e. The fluorescence images of stained L929 cells after 48 h of culturing show the distribution of cells along the patterned substrate. By comparing Fig. 9a–c and d–f, it can be concluded that cells can grow on and attach to the fabricated patterned substrates, as cells aggregated in the bottom of the stripe and lattice substrates. Microstructures can induce cell proliferation along the patterned surfaces, and different patterns can guide different cell distribution.

However, different from original distribution, cells distributed dispersedly and grew out gradually after 48 h; thus, cell growth was not as strict as the strip patterned substrate. The reasons why after 48 h cells tended to grow more irregularly are explained as follows. When cells change from spheroidal type to spindle type, they become more evenly distributed. The transition of fibroblasts morphology adhered to the substrate is from a spherical phenotype to a spindle, and cell migration requires basic adhesion. As a result,

spindle cells migrate faster than spherical cells that result in a uniform distribution of fibroblasts. The patterned valley was not deep enough to prevent cells from growing on the "wall." In addition, patterned substrates may have weak cell adhesion, which leads to the change in cell location.

Conclusions

In summary, this work developed a microfluidic device, which employed the biocompatible patterned microstructures to enhance cell proliferation and distribution. The patterned microstructures were fabricated using the SSAW-assisted fabrication method. The working principle and process of SSAW-assisted patterned microstructure fabrication method are investigated, and the results demonstrated that the undulate stripe and lattice patterned microstructures can be successfully fabricated, and the morphologies of the patterned microstructures can be adjusted by selecting the pairs of IDTs and the wavelength of SAW. The L929 cell seeding experiments on the developed microfluidic device showed that dynamic cell culturing has advantages for cell proliferation viability compared to static cell culturing. The stripe and lattice patterned microstructures can induce cell distribution along the valleys and wells, and different patterns can guide the corresponding different cell distributions.

For future work, more experiments will be performed to investigate the effects of patterned microstructures on guiding cell proliferation and distribution, including the width and amplitude. Also, we will pay more attention to organoids forming, like multi-types of cells could be cultured together to show its in vivo functionality. For the elongation and alignments of the cell, we will focus more on mimic of fiber-like tissue regeneration. Besides, the aggression of cells could be helpful in organoid functionality.

Acknowledgements The authors acknowledge the funding support from the National Natural Science Foundation of China (U1809220), Zhejiang Provincial Funds for Distinguished Young Scientists of China (LR19E050001), Open Fund Project of Zhijiang Laboratory (2019MC0AB02), Fund for Creative Research Groups of National Natural Science Foundation of China (51821093).

Compliance with ethical standards

Conflict of interest The authors declare that there is no conflict of interest.

Ethical approval This study does not contain any studies with human or animal subjects performed by any of the authors.

References

1. Fang Y, Eglen RM (2017) Three-dimensional cell cultures in drug discovery and development. SLAS DISCOVERY Adv Sci Drug Discov 22(5):456–472
2. Huh D, Matthews BD, Mammoto A, Montoya-Zavala M, Hsin HY, Ingber DE (2010) Reconstituting organ-level lung functions on a chip. Science 328(5986):1662–1668
3. Limongi T, Tirinato L, Pagliari F, Giugni A, Allione M, Perozziello G, Candeloro P, Di Fabrizio E (2017) Fabrication and applications of micro/nanostructured devices for tissue engineering. Nano-Micro Lett 9(1):1–13
4. Bhise NS, Manoharan V, Massa S, Tamayol A, Ghaderi M et al (2016) A liver-on-a-chip platform with bioprinted hepatic spheroids. Biofabrication 8(1):014101–014112
5. Toh YC, Lim TC, Tai D, Xiao G, Van Noort D, Yu H (2009) A microfluidic 3d hepatocyte chip for drug toxicity testing. Lab Chip 9(14):2026–2035
6. Zhang C, Zhao Z, Abdul Rahim NA, Van Noort D, Yu H (2009) Towards a human-on-chip: culturing multiple cell types on a chip with compartmentalized microenvironments. Lab Chip 9(22):3185–3192
7. Wei G, Ma PX (2004) Structure and properties of nano-hydroxyapatite/polymer composite scaffolds for bone tissue engineering. Biomaterials 25(19):4749–4757
8. Ma X, Qu X, Zhu W, Li YS, Yuan S, Zhang H, Liu J, Wang P, Lai CSE, Zanella F, Feng GS, Sheikh F, Chien S, Chen SC (2016) Deterministically patterned biomimetic human IPSC-derived hepatic model via rapid 3d bioprinting. Proc Natl Acad Sci 113(8):2206–2211
9. Lind JU, Busbee TA, Valentine AD, Pasqualini FS, Yuan H, Yadid M, Park SJ, Kotikian A, Nesmith AP, Campbell PH, Vlassak JJ, Lewis JA, Parker KK (2017) Instrumented cardiac microphysiological devices via multimaterial three-dimensional printing. Nat Mater 16(3):303–308
10. Qin D, Xia Y, Whitesides GM (2010) Soft lithography for micro- and nanoscale patterning. Nat Protoc 5(3):491–502
11. Mathew R, Sundaram MM (2012) Modeling and fabrication of micro tools by pulsed electrochemical machining. J Mater Process Technol 212(7):1567–1572
12. Kaufmann T, Gokmen MT, Rinnen S, Arlinghaus HF, Du Prez F, Ravoo BJ (2012) Bifunctional janus beads made by "sandwich" microcontact printing using click chemistry. J Mater Chem 22(13):6190–6199
13. Tang Y, Tan WK, Fuh JYH, Loh HT, Wong YS, Thian SCH, Lu L (2007) Micro-mould fabrication for a micro-gear via vacuum casting. J Mater Process Technol 192:334–339
14. Siqueira G, Kokkinis D, Libanori R, Hausmann MK, Gladman AS, Neels A, Tingaut P, Zimmermann T, Lewis JA, Studart AR (2017) Cellulose nanocrystal inks for 3d printing of textured cellular architectures. Adv Funct Mater 27(12):1604619-10
15. Yang Y, Chen Z, Song X, Zhang Z, Zhang J, Shung KK, Zhou Q, Chen Y (2017) Biomimetic anisotropic reinforcement architectures by electrically assisted nanocomposite 3d printing. Adv Mater 29(11):1605750
16. Zhang B, Luo Y, Ma L, Gao L, Li Y, Xue Q, Yang H, Cui Z (2018) 3D bioprinting: an emerging technology full of opportunities and challenges. Bio-Des Manuf 1(1):2–13
17. Chung JY, Naficy S, Yue Z et al (2013) Bio-ink properties and printability for extrusion printing living cells. Biomater Sci 1(7):763–773
18. Alemán-Domínguez ME, Ortega Z, Benitez AN, Monzón M, Garzón LV, Ajami S, Liu C (2018) Polycaprolactone–carboxymethyl cellulose composites for manufacturing porous scaffolds by material extrusion. Bio-Des Manuf 1(4):245–253

19. Xu T, Gregory C, Molnar P, Cui X, Jalota S, Bhaduri S, Boland T (2006) Viability and electrophysiology of neural cell structures generated by the inkjet printing method. Biomaterials 27(19):3580–3588
20. Jalvo B, Mathew AP, Rosal R (2017) Coaxial poly(lactic acid) electrospun composite membranes incorporating cellulose and chitin nanocrystals. J Membr Sci 544:261–271
21. Lu L, Tang X, Hu S, Pan Y (2018) Acoustic field-assisted particle patterning for smart polymer composite fabrication in stereolithography. 3D Print Addit Manuf 5(2):151–159
22. Ding X, Lin SC, Kiraly B, Yue H, Li S, Chiang IK, Shi J, Benkovic SJ, Huang TJ (2012) On-chip manipulation of single microparticles, cells, and organisms using surface acoustic waves. Proc Natl Acad Sci 109(28):11105–11109
23. Hu J, Hardy C, Chen CM, Yang S, Voloshin AS, Liu Y (2014) Enhanced cell adhesion and alignment on micro-wavy patterned surfaces. PLoS ONE 9(8):e104502
24. HahnMS Taite LJ, Moon JJ, Rowland MC, Ruffino KA, West JL (2006) Photolithographic patterning of polyethylene glycol hydrogels. Biomaterials 27(12):2519–2524
25. Meng B, Deng J, Liu Q, Wu Z, Yang W (2012) Transparent and ductile poly(lactic acid)/poly(butyl acrylate) (pba) blends: structure and properties. Eur Polym J 48(1):127–135
26. Nguyen KT, West JL (2002) Photopolymerizable hydrogels for tissue engineering applications. Biomaterials 23(22):4307–4314
27. Fairbanks BD, Schwartz MP, Bowman CN, Anseth KS (2009) Photoinitiated polymerization of peg-diacrylate with lithium phenyl-2,4,6-trimethylbenzoylphosphinate: polymerization rate and cytocompatibility. Biomaterials 30(35):6702–6707
28. Tuncaboylu DC (2018) Photo-crosslinked mechanically strong pcl 4-pdmaem hydrogels. React Funct Polym 126:44–51
29. Yin J, Yan M, Wang Y, Fu J, Suo H (2018) 3D bioprinting of low-concentration cell-laden gelatin methacrylate (gelma) bioinks with a two-step cross-linking strategy. ACS Appl Mater Interfaces 10(8):6849–6857
30. Mei D, Xue D, Wang Y et al (2016) Undulate microarray fabrication on polymer film using standing surface acoustic waves and ultraviolet polymerization. Appl Phys Lett 108(24):3038-4
31. Wang Y, Xue D, Mei D (2018) Patterned microstructure array fabrication by using a novel standing surface acoustic wave device. ASME J Micro Nano Manuf 6:21002–21007
32. Krishnamoorthy S, Zhang Z, Xu C (2020) Guided cell migration on a graded micropillar substrate. Bio-Des Manuf 3:60–70